AGU Advances

RESEARCH ARTICLE
10.1029/2021AV000398

Key Points:

- Passive seismic interferometry reveals detailed insights into subsurface water storage variability in the Nepal Himalayas
- Vadose zone moisture saturation controls river discharge generation in a steep mountain landscape
- Freshwater delivery from high mountains is strongly dependent on subsurface conditions, which are rarely considered in these environments

Supporting Information:

Supporting Information may be found in the online version of this article.

Correspondence to:

L. Illien,
lillien@gfz-potsdam.de

Citation:

Illien, L., Andermann, C., Sens-Schönfelder, C., Cook, K. L., Baidya, K. P., Adhikari, L. B., & Hovius, N. (2021). Subsurface moisture regulates Himalayan groundwater storage and discharge. *AGU Advances*, *2*, e2021AV000398. https://doi.org/10.1029/2021AV000398

Received 20 JAN 2021
Accepted 31 MAR 2021

Author Contributions:

Conceptualization: L. Illien, C. Andermann, C. Sens-Schönfelder, N. Hovius
Data curation: L. Illien, C. Andermann, C. Sens-Schönfelder, K. P. Baidya, L. B. Adhikari
Formal analysis: L. Illien, C. Andermann
Investigation: L. Illien, C. Andermann, C. Sens-Schönfelder, K. L. Cook, N. Hovius
Supervision: C. Andermann, C. Sens-Schönfelder, N. Hovius

Subsurface Moisture Regulates Himalayan Groundwater Storage and Discharge

L. Illien[1,2], C. Andermann[1], C. Sens-Schönfelder[1], K. L. Cook[1], K. P. Baidya[3], L. B. Adhikari[4], and N. Hovius[1,2]

[1]Helmholtz Center, German Research Center for Geosciences GFZ, Potsdam, Germany, [2]Department of Geosciences, University of Potsdam, Potsdam, Germany, [3]Department of Hydrology and Meteorology, Kathmandu, Nepal, [4]Department of Mines and Geology, Kathmandu, Nepal

Abstract Through the release of groundwater, most mountain rivers run year-round despite their small catchments and sporadic precipitation. This makes mountain ranges important sources of reliable freshwater for downstream populations in many parts of the world. However, due to a lack of ground instrumentation, little is known about groundwater dynamics in mountainous landscapes. Recent research has shown that the amount of moisture trapped in the soil and weathered rocks in the vadose zone can significantly buffer groundwater recharge and runoff but the wider recognition of this effect on major mountain systems has not been yet established. In this study, we test whether the moisture reservoir has an impact on hydrological fluxes in a steep Himalayan catchment during three monsoon seasons. We measured an array of parameters including relative seismic velocity changes from ambient noise correlations. This noninvasive technique allows us to monitor groundwater dynamics in conjunction with classical hydrological measurements. We found that the moisture saturation in the vadose zone controls the onset of groundwater recharge and runoff and therefore determines the annual water availability supplied by monsoon precipitation. We model this dynamic using a surface layer that has a finite storage capacity that controls the connectivity of surface flux to groundwater. The extension of this concept, which is thought to apply widely in flat and undulating landscapes, to steep mountain topography with thin and discontinuous soils underlain by regolith and bedrock has important implications for mountain hydrology.

Plain Language Summary The Nepal Himalayas supply essential water resources to a large part of the population of South Asia. Most of this water drains through a mountain groundwater reservoir that is poorly constrained. In steep landscapes, this reservoir is continuously losing water due to gravitational pull. Understanding how the reservoir fills and drains is crucial to the assessment of its sustainability and projection into the future with respect to global climate change. However, the relevant subsurface processes are generally challenging to observe due to limited access to the subsurface, particularly in steep mountain landscapes. We have used seismic ambient noise, ground vibrations continuously recorded by seismometers, to monitor the groundwater dynamics on a spatially integrated scale in a Himalayan valley. We show that the moisture content of a shallow layer controls the transfer of precipitation into the deeper groundwater reservoir during the Indian monsoon seasons. Our study highlights the need to anticipate the effects of changes of land use, soil cover conditions and rainfall regime, due to climate change, to better predict the future of freshwater resources in mountain landscapes.

1. Introduction

The fate of water in mountains involves flow pathways through reservoirs with different physical properties and capacities (Alley et al., 2002; Oki & Kanae, 2006). Accurate water budget estimation requires knowledge of these reservoirs and their connections, specifically of groundwater storage dynamics in response to precipitation inputs and its export to discharge. Most water in rivers has an age of years to decades (Gleeson et al., 2016; McGuire & McDonnell, 2006), which suggests that it has spent a significant amount of time in storage. This "old" water concept is especially relevant in steep mountain catchments, where deeper vertical infiltration seems more prevalent than direct runoff (Jasechko et al., 2016). It is widely accepted that these mountain areas act as water towers that supply essential fresh water resources downstream. The prime example is the Himalayan Range, which provides water for ~800 million people in the Indus, Ganges,

Writing – original draft: L. Illien
Writing – review & editing: L. Illien, C. Andermann, C. Sens-Schönfelder, K. L. Cook, N. Hovius

and Brahmaputra basins. The evolution of this resource is often viewed through the prism of glacier melt (Immerzeel et al., 2010; Viviroli et al., 2007), whereas the larger and more ubiquitous mountain groundwater reservoir has received less attention. With ∼2/3 of the annual river discharge in the Nepal Himalayas coming from groundwater (Andermann et al., 2012), understanding the key controls on this reservoir is essential for projecting the future of mountain water resources in the light of global climate change and increasing hydropower and land use. However, constraints on groundwater recharge and dynamics in this area and more generally in mountainous landscapes are rare due to the scarcity of ground observations in steep remote locations.

Before reaching groundwater and ultimately streams, precipitation must generally first pass through the unsaturated superficial zone of the subsurface (vadose zone), which suggests that any change in physical conditions within this shallow layer may modulate groundwater recharge and runoff. In steep catchments, the importance of this conditioning for controlling hydrological fluxes is often debated due to the lack of instrumentation and contradicting observations. A first string of studies have shown that hydrological fluxes in steep catchments are mainly controlled by the presence of a fractured bedrock basement in these locations that promotes fast flow and efficient infiltration to the groundwater table, therefore quickly bypassing the vadose zone (Andermann et al., 2012; Katsura et al., 2008; Padilla et al., 2014, 2015; Salve et al., 2012; Zillgens et al., 2007). This preferential flow path along fractures has been reported to cause an important volumetric contribution of bedrock groundwater to both the baseflow and stormflow component of discharge in these studies. This observation could also explain the weak dependence of groundwater recharge and runoff dynamics with subsurface conditions and the soil/sediment cover (Padilla et al., 2014, 2015; Salve et al., 2012). Nevertheless, a few studies have also shown that hydrograph response to precipitation is dependent on initial baseflow and various preconditions in the vadose zone. Such preconditions include current soil wetness that determines soil hydrological conductivity (Tani, 1997) or a finite water storage capacity in the regolith which modulates the transfer of precipitation to rivers and to deeper reservoirs (Montgomery et al., 1997; Onda, 1989). Recent research has shown that a significant volume of water stored in the regolith is in fact "rock moisture" that is trapped below the soil layer in the unsaturated weathered layer of bedrock (Rempe & Dietrich, 2018; Salve et al., 2012). In this study, we will use the term subsurface moisture reservoir for all exchangeable water in the vadose zone, encompassing soil and rock moisture. Because this reservoir can represent a significant part of seasonal dynamic storage (Dralle et al., 2018) and is located above the groundwater table, it has been shown to buffer groundwater recharge by precipitation and hinder runoff in a steep (32°) 4 km^2; hillslope in the Northern California Coast Ranges (Rempe & Dietrich, 2018). However, a very limited effect of subsurface moisture on groundwater storage and discharge has also been reported close to the same study site due to the previously mentioned fracture pathways (Salve et al., 2012). This discrepancy in the literature raises the question of the relevance of the subsurface moisture for regulating water transfers at larger scales, as this control is generally observed locally on rather small hillslopes. In this study, we hypothesize that the highly variable conditions in subsurface moisture due to the monsoon seasonality in the Nepal Himalayas regulate groundwater recharge and runoff generation at the catchment scale and thus control the annual availability of hydrological resources downstream.

To track subsurface water in a spatially integrated way in remote locations where standard techniques and data may be limited, new approaches are needed for monitoring groundwater dynamics. Here, we use noninvasive seismic interferometry, based on data from broadband seismometers. From ambient seismic noise correlations, seismic interferometry retrieves relative seismic velocity changes (dv/v) in the subsurface, allowing for the monitoring of rock properties through time (Gassenmeier et al., 2016; Lobkis & Weaver, 2001; Sens-Schönfelder & Wegler, 2006). Because fluid content in rocks affects elastic moduli and therefore seismic velocity, seismic interferometry can be used to estimate relative groundwater storage evolution (Clements & Denolle, 2018; Kim & Lekic, 2019; Lecocq et al., 2017; Sens-Schönfelder & Wegler, 2006). This method is sensitive at the mesoscale (10^1–10^2 m, length scale of the 3D volume of influence), allowing for spatially integrated monitoring of the groundwater system and its dynamics. Thus, it bridges the gap between point-based well measurements and larger scale methods such as catchment scale hydrograph analysis or satellite-based gravimetry. It also avoids possible observational artifacts compared to piezometric measurements, where borehole installation often alters the subsurface condition.

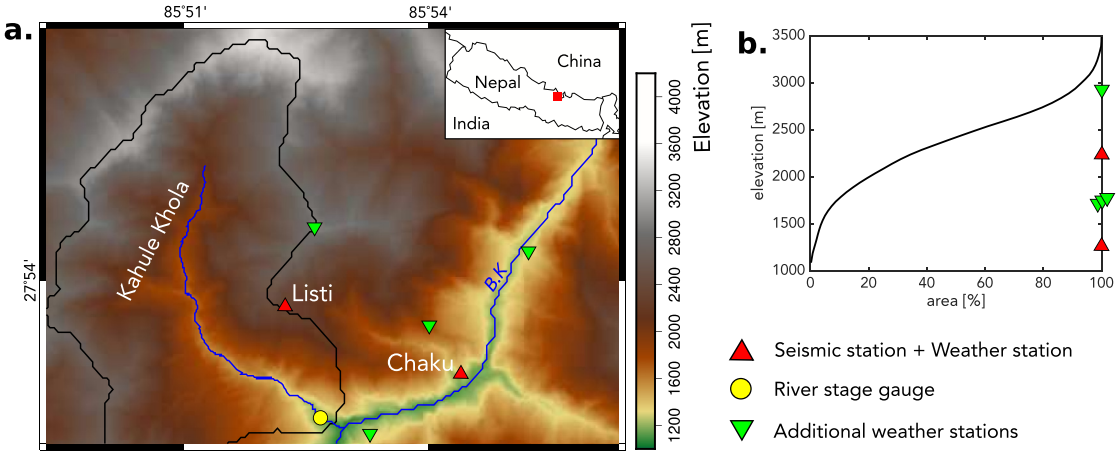

Figure 1. (**a.**) Map showing the Bhote Koshi observatory. Red triangles indicate the sites that contain seismic stations, soil moisture sensors and precipitation gauges. Yellow circle in the Kahule Khola tributary indicates the hydrometric station where stage height and $\delta^{18}O$ are measured. Green triangles are additional weather stations used for estimating average precipitation. Red square in inset shows location of the observatory in Nepal. BK: Bhote Koshi river. (**b.**) Hypsometric curve of the Kahule Khola catchment. Symbols on the right axis of the plot represent the elevation of the stations relatively to the Kahule Khola hypsometry.

We have used seismic interferometry to study groundwater dynamics in the Himalayas, focusing on the Bhote Koshi catchment in Nepal (Figure 1a). Like most catchments in the central Himalaya, the Bhote Koshi receives up to ~80% of its annual precipitation during the Indian Summer Monsoon (Bookhagen & Burbank, 2010). We analyzed ~2.5 years of seismic data, covering three monsoon seasons, recorded at two seismic stations (Figure 1a). Listi station was located at 2,310 masl., near a ridge crest with steep flanks (slope of ~80%), and ~1,100 m above the Chaku station, which was located on a bedrock terrace 75 m above the Bhote Koshi River. Both stations are underlain by sheared metasedimentary rocks of the Lesser Himalayan series, below a layer of regolith and colluvium. To resolve interactions between precipitation, subsurface moisture, groundwater, and river discharge in this typical mountain setting, we combined the observations from these stations with complementary measurements (Figure 1a). Soil moisture sensors installed in the surface layer (0–20 cm depth) were located at both seismic stations and precipitation was measured at six weather stations. In addition, we measured the flow stage height of the Kahule Khola upstream of its confluence with the Bhote Koshi River using a pressure sensor. This stream drains a ~35 km^2, glacier-free catchment, the flow of which reflects the drainage of the instrumented ridge by which it is bounded. At the stage gauge, stream water samples were taken twice a week from January 2016 to October 2018. The stable oxygen isotope ratio ($\delta^{18}O$) of these samples was measured as a tracer for seasonal water input variations and to probe for evaporative loss. Finally, we extracted the normalized difference vegetation index (NDVI) from MODIS multi spectral imagery. NDVI is generally correlated with soil moisture (Taktikou et al., 2016) and is a good proxy for vegetation activity and transpiration (Ichii et al., 2010; Running & Nemani, 1988). This multi-proxy approach allowed us to assess the temporal evolution of groundwater storage, and revealed the first-order importance of subsurface moisture in regulating groundwater recharge and baseflow release during the monsoon in the Nepal Himalayas.

2. Materials and Methods

Precipitation was measured at six locations using fully automated VAISALA WXT510 Weather Transmitters (Figure 1a). All weather parameters were logged at 1-min intervals. To obtain a representative time series and account for potential orographic effects, all six precipitation measurements were interpolated in a square box extending ~10 × 10 km by applying a Voronoi-Thiessen tessellation on the daily precipitation sums (Figure S1). The aggregated precipitation time series represents the spatial mean precipitation of the integration area. Stations with missing data at certain dates were not used for spatial interpolation. We used the dirichlet(X) function in the R spatstat package. Because most of the Kahule Khola catchment lies under 3,000 m altitude (Figure 1b), snowfall is neligible at our field site (Putkonen, 2004).

Relative river stage height of the Kahule Khola river was measured ~100 m upstream of the confluence with Bhote Koshi River (Figure S1). Stage height was logged using Hobo Onset pressure transducers. The logging interval was set to either 15 or 30 min intervals depending on the deployment period. The relative stage height record was corrected for atmospheric variations using the barometric time series recorded at our closest weather station, Tyantali station (Figure S1).

For the measurement of $\delta^{18}O$, daily water samples were taken by a trained onsite operator every day at around 9 a.m. Sampler were filtered onsite (0.22 μm filter) and stored in 30 ml Nalgene vials at ambient temperature before being shipped to Germany. All samples were analyzed in the GFZ Potsdam OSG-Lab, using a Picarro L-2140i Ringdown spectrometer.

Soil moisture was acquired at the six weather stations using a Campbell Scientific CS650 soil moisture sensor. The sensor was installed close to the surface and integrates approximately 8 liters of soil volume and records volumetric water content as a function of bulk electric conductivity.

NDVI was extracted from the online MODIS/VIIRS Land Products global Subsetting Tool. The subsetting area was picked to cover the entire Kahole Kohla landscape to integrate valley-to-ridge variability of vegetation types and agricultural land use. The Tool is available at https://modis.ornl.gov/globalsubset/.

Broadband seismic stations (Nanometrics - Trillum Compact 120s) were used in this study. Data were acquired at a sampling rate of 200 Hz. We estimated daily relative seismic velocity changes from ambient seismic noise correlations in the frequency range of 4–8 Hz. We used single-station cross correlation technique (Hobiger et al., 2014) and computed the velocity time series from the stretching method using multiple references (Sens-Schönfelder & Wegler, 2006; Sens-Schönfelder et al., 2014). Detailed method is available in Appendix A.

3. Results and Discussion

3.1. Co-Evolution of Hydrological Variables

The Indian Summer Monsoon imposes a strong annual cycle on the hydrology of the Bhote Koshi catchment, with a distinct dry and wet season (Figure 2a). The seasonality of precipitation input is matched by a sustained increase in discharge of the Kahule Khola stream during the monsoon, followed by a well-defined long-lasting recession throughout the dry part of the year. Importantly, we observed little to no discharge generation in the pre-monsoon season (~March to ~June). Despite significant precipitation in the pre-monsoon season, the hydrograph shows a continuous decrease in baseflow-generated river discharge with only a few short-lived rise-and-fall type events from direct runoff. This decoupling suggests that there are different hydrological regimes throughout the year. Because the stream is predominantly fed by groundwater (Andermann et al., 2012), the transition between these regimes is likely to be controlled by the onset of groundwater recharge, initiating a period when groundwater and precipitation are coupled. If this is correct, then understanding the timing of this coupling in relation to precipitation input is essential, requiring observation of groundwater storage through time. We defined two seasonal boundaries based on this coupling in Figure 2: from a dry to an uncoupled-wet season and from an uncoupled-wet to a coupled-wet season.

Previous work has linked seismic velocity decreases to increased groundwater levels (Clements & Denolle, 2018; Kim & Lekic, 2019; Lecocq et al., 2017; Sens-Schönfelder & Wegler, 2006) and increases in pore pressure (Q.-Y. Wang et al., 2017). Thus, the time series of estimated daily relative seismic velocity changes dv/v at Listi and Chaku stations (Figure 2b) may serve as a relevant proxy for groundwater storage. The annual cyclicity of dv/v, with a decrease during each recorded monsoon seasons followed by a recovery during the subsequent dry season is in agreement with these studies. At ~8%, the amplitude of change at our stations was significantly larger than in previously reported cases (Clements & Denolle, 2018; Kim & Lekic, 2019; Lecocq et al., 2017), suggesting a dominant hydrological forcing on the velocity changes through substantial variations in groundwater content and level. Both stations exhibited similar dv/v dynamics, with a lower amplitude at Listi. This amplitude difference could reflect smaller groundwater variations at Listi because it is at a higher topographic position with less upstream area. However, because the seismic interferometry technique loses sensitivity to changes with increasing depth (Obermann et al., 2013; Pacheco & Snieder, 2005), our observations could also point to a deeper average groundwater level higher

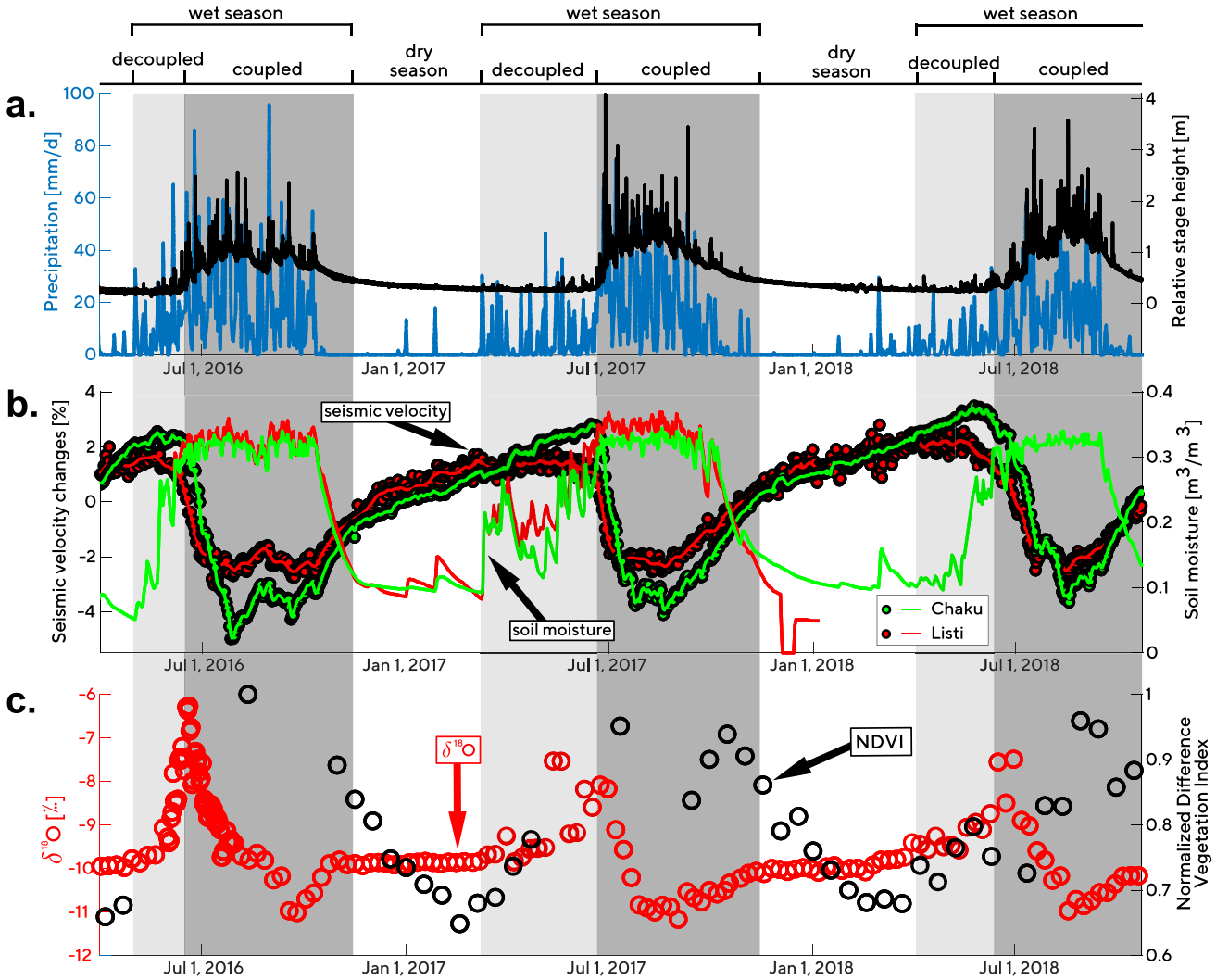

Figure 2. Observations from the Bhote Koshi observatory (**a.**) Black solid line indicates the river stage height measured at the Kahule Khola. Daily precipitation is plotted in blue. (**b.**) Daily relative seismic velocity changes variations in the 4–8 Hz frequency band is plotted as circles with a 3 days moving average for visualization. Measurements of soil moisture volumetric content are reported by the solid lines. Green and red colors indicate Chaku and Listi sites respectively. (**c.**) Red dots represent $\delta^{18}O$ values measured at the Kahule Khola. Black Dots represents Normalised Difference Vegetation Indexes (NDVI) computed in our study area, that is a proxy for vegetation activity. The different seasons and regimes of the hydrological system are indicated in the background and labeled at the top.

in the landscape (Jasechko et al., 2016). A striking co-evolution between the streamflow (Figure 2a) and the dv/v time series occurred during major parts of the monitored period: the variables were negatively correlated during monsoons, and the recovery of velocities during the post-monsoon period coincided with a discharge recession. Remarkably, the sharp decrease of seismic velocity during the monsoon systematically coincided with a sustained increase in streamflow.

Further insight into the timing of this onset and the fate of pre-monsoon precipitation comes from soil moisture measurements (Figure 2b). Over the annual cycle, the measured soil moisture concentration had a pronounced relation with precipitation (Figures 2a and 2b). From the onset of pre-monsoon precipitation, soil moisture increased, while dv/v remained unaffected, suggesting that any infiltrating rainwater was stored in the shallow subsurface unconnected to the groundwater. The onset of coupling of precipitation and groundwater occurred around the start of the summer monsoon, after reaching ~610, 660, and 400 mm of cumulative precipitation in 2016, 2017, and 2018, respectively. Coupling coincided with the stabilization of soil moisture concentrations, despite mounting precipitation totals. We attribute this stabilization to

reaching a mean field capacity of the vadose zone. Under these conditions, the equivalent volume of any additional water input to the subsurface is gravitationally transferred into the groundwater reservoir, leading to rising groundwater levels reflected by the seismic velocity decrease. We note that the buildup of moisture in the subsurface during the pre-monsoon period was barely recorded by the seismic velocity observations (Figure 2b). This may be due to the frequency-dependent response of velocity changes to partial fluid content (Helle et al., 2003; White, 1975), or to the limited depth extent of the layer prone to soil moisture changes. The duration of the soil moisture buildup phase was different for the three seasons on record with different cumulative precipitation totals, likely because of differences in precipitation intensity. In addition, transpiration losses could have slowed the increase in moisture. The onset of vegetation activity signaled by increasing NDVI values during the pre-monsoon period underpins this interpretation (Figure 2c).

The co-evolution of our hydrological observables gives insight into the transition from the coupled to the uncoupled hydrological regimes after the monsoon season. Early in the dry season, a distinct and sustained decrease in the rate of recovery of dv/v occurred in both recorded years (Figure 2b), especially visible at Chaku station. This change of slope suggests a step change in groundwater depletion, from fast in the early post-monsoon to steady, but slower depletion during the dry season from ~November until around the start of the next monsoon. Because this feature follows the last monsoon precipitation and the decrease in soil moisure, we used it to conservatively define the end of the wet season (boundary between the wet-coupled to dry season in Figure 2). We note that the stage height of the Kahule Khola does not share the slope break observed in dv/v. This hints at the operation of a second groundwater depletion pathway, connected not to streamflow, but rather upwards via transpiration, which operates during the coupled hydrological regime, but not during the subsequent dry season. This hypothesis can be tested with the oxygen isotope record of the Kahule Khola.

Over the monitoring period, which comprised two annual cycles, $\delta^{18}O$ values of Kahule Kohla discharge were constant around −10‰ during the dry season, increased progressively to −6‰ from the onset of pre-monsoon precipitation, dropped rapidly to around −11‰ early in the monsoon season, and restored to values around −10‰ later in that season (Figure 2c). The stable isotopic composition of stream water is determined by the precipitation input and any subsequent fractionation. We constrain precipitation chemistry using a contemporaneous precipitation $\delta^{18}O$ measurement time series of samples from Kathmandu (Figure S7). Kathmandu is located at 1,400 masl., about 50 km to the SW of our study area, and exposed to the same general weather systems. During 2016 and 2017, Kathmandu precipitation $\delta^{18}O$ showed a similar pattern, with sparse dry season values around −9‰, pre-monsoon values increasing up to 5‰, early monsoon rain around −15‰ increasing to −10‰ later in the monsoon season. Fractionation after precipitation appears to be limited, as the Kahule Khola $\delta^{18}O$ data consistently plot on a local meteoric waterline (Figure S6).

In this context, and in view of the paucity of winter precipitation, we interpret the constant, intermediate $\delta^{18}O$ values for Kahule Khola dry season water samples to indicate that the stream was mainly fed by a groundwater reservoir in which isotopically light monsoon input is mixed with some isotopically heavier pre-monsoon input on time scales exceeding an annual cycle. It is likely that this mixing occurs after the vadose zone has reached field capacity and water starts to move downward into the groundwater reservoir. Heavier isotopic values of Kahule Khola stream water indicate that a part of pre-monsoon rainfall translates into fast direct runoff. At the onset of the coupled hydrological regime, with incoming isotopically light monsoon precipitation, the oxygen isotopic values of the stream water decreased to slightly below the characteristic value of the groundwater reservoir. We attribute this to a combination of groundwater evacuation and direct runoff during intense monsoon rainfall. The Kahule Khola water reverted to its steady, well-mixed $\delta^{18}O$ signature independently of the slope break in the dv/v time series at Chaku, early in the post-monsoon dry season. We infer that the secondary, upward loss of water in the period before the break is largely due to vegetation transpiration which can modulate the drainage of water tables close to rooting depth (Koirala et al., 2017; Maxwell & Condon, 2016) without oxygen isotope fractionation.

3.2. Soil Moisture and Groundwater Recharge

Our results suggest that two distinct hydromechanical regimes are active in the steep Kahule Khola catchment. A key parameter controlling the passage between these regimes could be the pore connectivity in the

vadose zone. When this zone is undersaturated, the pores are not efficiently connected and the presence of air may impede flow, causing infiltrated rainwater to be stored as tightly bound water (Renée Brooks et al., 2010) that is removed by root uptake building up early season biomass. This state is characterized by short-lived episodes of direct runoff generation and a continuous decrease of baseflow. When the subsurface moisture reservoir reaches a characteristic storage capacity, the subsurface can no longer store additional water and begins to transmit to the deeper groundwater reservoir. This behavior is analogous to a "sponge" where prior hydrophiling of the surfaces modulates the infiltration (DiCarlo, 2004, 2006). After the monsoon, the bound water depleted by transpiration can be replaced by groundwater through upward percolation processes (Renée Brooks et al., 2010), allowing vegetation to use groundwater indirectly at depths exceeding the root zone (Condon et al., 2020; Koirala et al., 2017). Therefore, evapotranspiration of subsurface moisture competes directly with precipitation input to regulate groundwater recharge. Because we cannot differentiate between a shallow and deep groundwater reservoir at our field site, the hypothesis of a perched seasonal groundwater reservoir (Padilla et al., 2015; Salve et al., 2012) depleted by transpiration is also plausible. Therefore, the dynamics would be an integrated measure of both shallow and deep groundwater storage. We conclude that despite evidence for a fractured bedrock basement in the Nepal Himalayas (Andermann et al., 2012; Tipper et al., 2006), the subsurface moisture reservoir governs hydrological fluxes in the Kahule Khola.

While this concept explains our observations at Chaku station, low in the Bhote Koshi valley, it may not apply to higher positions in the mountain landscape. At Listi station, close to a mountain ridge crest, seismic velocities decreased somewhat during pre-monsoon despite the soil moisture not being at saturation, suggesting that precipitation became connected to the groundwater reservoir (Figures 2a and 2b). This early connection may be due to a greater permeability of the surface, associated with thin soil cover and the presence of deep-reaching tension fractures that allows localized areas of rapid recharge (Gleeson et al., 2009). Moreover, the clear slope break that we attribute to the termination of transpiration losses from the groundwater reservoir at Chaku is not as striking at Listi, where the recovery in dv/v appeared more gradual from the wet to the dry season. This can be explained by a groundwater reservoir that is below rooting depth (Maxwell & Condon, 2016). The similar but yet different seismic velocity evolution at Listi and Chaku shows that the seismic interferometry approach is a promising tool to monitor groundwater dynamics in different parts of a landscape, including those that may be representative of the catchment and its subsurface. Thus, local gradients in the groundwater system can be targeted, something that is beyond the reach of classic hydrograph analysis.

3.3. Modeling of Seismic Velocity Changes

Our data suggest that subsurface moisture is a first-order control on groundwater storage and discharge in the Himalayan Bhote Koshi catchment. We further demonstrate our findings by reproducing the dv/v data with a hydrological model.

Simple hydrological models have succeeded in reproducing key features of dv/v variation in various settings (Gassenmeier et al., 2015; Hillers et al., 2014; Sens-Schönfelder & Wegler, 2006). Although the details of these models have varied, they shared the assumption of instantaneous transfer of precipitation to the groundwater system on the daily timescale. Such models predict an exponential decay of the modeled hydrological variable (evolution of groundwater table level, pore pressure, groundwater storage) after precipitation input. To test whether these models can capture the essence of groundwater hydrology at our field site, we have tried to fit the velocity changes observed at Chaku station with a groundwater-level evolution model (Hillers et al., 2014; Sens-Schönfelder & Wegler, 2006). We computed the hydraulic head $h(t)$ as follows:

$$\frac{dh}{dt} = \frac{P(t)}{\phi} - ah(t) \tag{1}$$

where P is the daily precipitation measured at the site, ϕ is the porosity of our reservoir, and a is a decay parameter that describes the recession of the hydraulic head after precipitation. We then converted changes in hydraulic head $h(t)$ into synthetic relative seismic wave velocity changes, by linking the relative variation

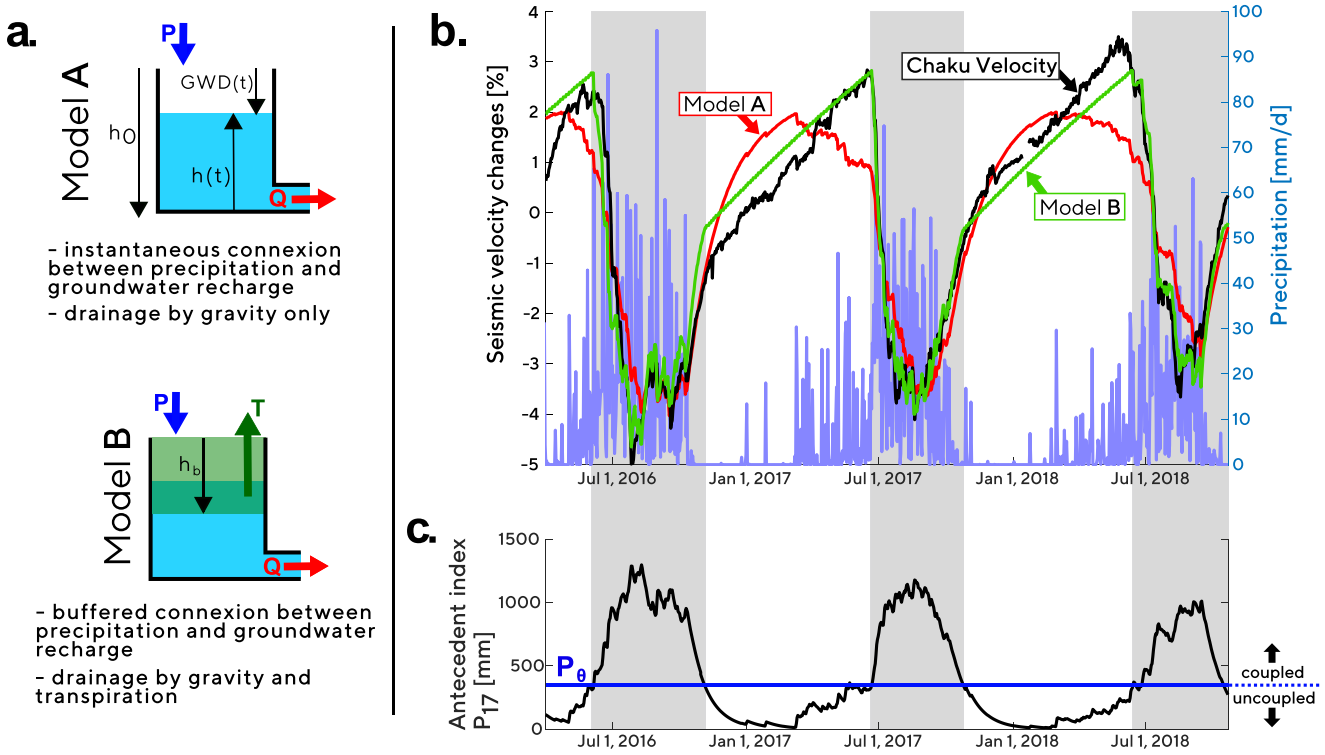

Figure 3. Results of dv/v modeling (**a.**) The sketches indicate models tested in the paper with sign conventions shown by black arrows. Colored arrows accounts for the fluxes regulating groundwater dynamics (P: Precipitation, Q: Discharge, T: transpiration). GWD (Groundwater Depth), h (hydraulic head), h_0 (asymptotic level), and h_b (critical depth for transpiration) are the variables described in Equations 1 and 3. (**b.**) Observations from Chaku station and the best fitting dv/v predictions of models **A** and **B**. (**c.**) Antecedent precipitation index P_{17} used in model **B** and the P_θ threshold. Gray areas depict the periods when the groundwater is connected to precipitation and transpiration, for example, at the field capacity of the vadose zone when $P_{17} > P_\theta$.

in saturated rock mass with a relative slowness perturbation of the medium (details in Appendix B01). Results from this model do not adequately reproduce the Chaku data (Figure 3b). For example, the synthetic velocities decrease during the pre-monsoon, as model precipitation is directly passed to the groundwater reservoir (model **A**, Figure 3a). This model may be valid in places such as volcanoes (Sens-Schönfelder & Wegler, 2006) where highly permeable bedrock is exposed at the surface. However, in our setting, the subsurface moisture reservoir buffers groundwater recharge and may be represented by including a second layer in the model. To do this without introducing unconstrained physical quantities, we computed the antecedent precipitation index $P_M(t)$ (Katsura et al., 2008; Kosugi et al., 2008):

$$P_M(t) = P_M(t-1)\exp(\ln 0.5 \,/\, M) + R_h(t)\exp(\ln 0.5 \,/\, 2M). \tag{2}$$

Here, $R_h(t)$ is the cumulative precipitation from $t-1$ to t, and M the time in days required for precipitation input to the layer to decay to half its initial value. We assumed that the filling of the subsurface moisture reservoir can be represented by the cumulative nature of Equation 2 and that the half-time M captures the reduction of the moisture content by transpiration. Then, we introduced a threshold P_θ to represent the field capacity of the vadose zone. The P_θ threshold was taken as the mean value of $P_M(t)$ at the dates corresponding to the onset of the seismic velocity decrease between the uncoupled to coupled regimes in 2016, 2017 and 2018 (details in Appendix B02). Precipitation is only passed to the groundwater reservoir when $P_M(t) > P_\theta$ with

$$\frac{dh}{dt} = \frac{P(t)}{\phi} - ah(t) - b\,(\min(0, GWD(t) - h_b)) \tag{3}$$

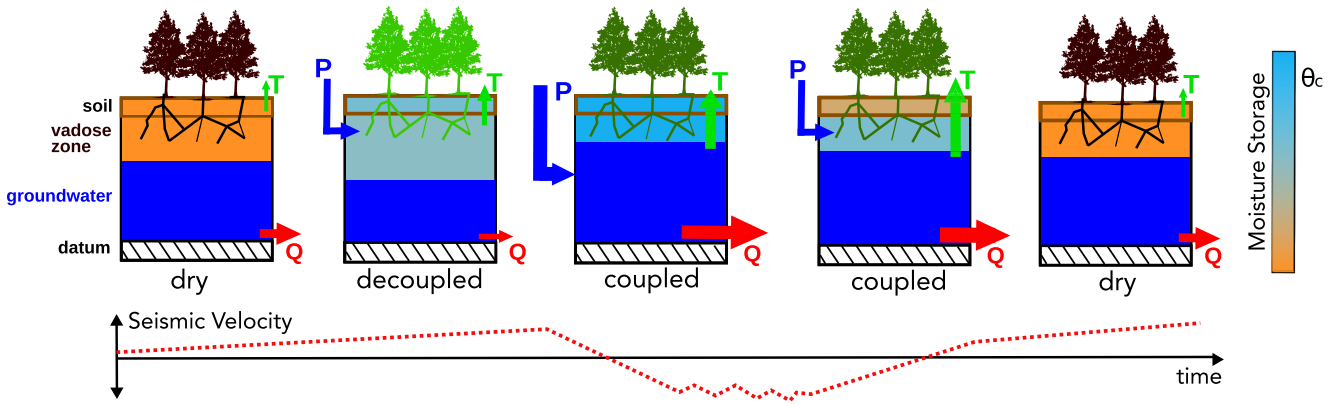

Figure 4. Conceptual sketch of the evolution of hydrological systems throughout the monsoon cycle. The arrows indicate the fluxes that control groundwater and subsurface moisture storage with T being transpiration, P the precipitation, and Q the discharge. The colorbar indicates the scale for subsurface moisture storage where θ_c is the characteristic field capacity required to connect the precipitation input and the transpiration outtake to the groundwater. Colors in trees indicate the evolving vegetation activity during one complete seasonal cycle. Sketches are in a 1D representation. Schematically, we also report the corresponding dv/v variations observed at Chaku at the different part of the Monsoon cycle. Time axis is not scaled.

where GWD(t) is the groundwater depth, and h_b is the depth range in which transpiration is active (model **B**, Figures 3a and 3b). b is a coupling constant linking the transpirative flux with the groundwater level through an increase of root density toward the surface (Canadell et al., 1996). This scaling is a simplification as water may be used directly and indirectly by roots. For periods with $P_M(t) < P_\theta$, we used Equation 1 without a precipitation input term. Our model best fits the seismic velocity data of Chaku station with (least-squares misfit criterion $L^2 = 0.022$, model **B** shown in Figures 3b and 3c), and M values from ~10 days to ~40 days produce reasonable fits (L^2 shown in Figure S5). We attribute this broad range of suitable half-time values to a lack of constraints in our model and to the simplicity of our approach.

A few offsets between our model and the data occurred during dry seasons, possibly due to changing local hydro-geological complexities, the single groundwater reservoir assumption, thermal strain (Richter et al., 2014), or a long term mechanical effect of the 2015 Gorkha earthquake and aftershocks on seismic velocity (Brenguier et al., 2008). In general, though, our modeling captures the dv/v dynamics and shows that key hydrological observations in the Bhote Koshi catchment require a subsurface moisture layer which is governed by the balance of precipitation input and transpirative loss, and acts as a gatekeeper that either separates the groundwater reservoir from surface precipitation or to permits recharge.

4. Conclusions and Perspectives

Based on our combined seismological, hydrological, meteorological, and geochemical observations and modeling, the precipitation-subsurface moisture-groundwater-stream water complex in the central Nepal Himalayas undergoes an annual cycle with four stages (Figure 4). (1. *Dry Stage*) The background is defined by a dry season, during which stream flow is fed only by gravity-driven groundwater discharge, causing progressive depletion of the groundwater reservoir. (2. *Decoupled Stage*) Pre-monsoon precipitation is converted to subsurface moisture and direct runoff, but does not result in groundwater recharge, such that the groundwater reservoir continues to be depleted. During this period, precipitation and groundwater are decoupled, and this state is prolonged by transpiration loss of subsurface moisture. (3. *Coupled Stage*) When the shallow subsurface, that is, the vadose zone, has reached field capacity, precipitation causes direct runoff as well as groundwater recharge and evacuation. During this coupled phase, when precipitation and groundwater are connected, moisture that accumulated in the vadose zone over the pre-monsoon season remains constant and additional precipitation is removed by transpiration or mixed with the pre-monsoon input and is moved into the groundwater reservoir at a rate determined by the local hydraulic conductivity and the infiltration capacity. Mixed water resides in this reservoir for at least one full annual cycle, meaning that evacuated mountain groundwater is older water. (4. *Coupled Stage*) As monsoon precipitation wanes, groundwater recharge slows down and a combination of evacuation to streams and upward loss through

transpiration causes the groundwater table to drop. This drop is initially fast, but slows down once plants are no longer connected to the groundwater reservoir. At this point, the dry state sets in anew.

The annual cycle we have described has hydrological seasons, which may differ from the meteorological seasons (Brunello et al., 2019; Müller et al., 2014). In the Nepal Himalayas, the crucial transition from the decoupled to the coupled state, after which precipitation is most effectively translated into runoff, is determined by the saturation of the subsurface, which is governed, in turn, by the balance of precipitation and evapotranspiration during the preceding weeks to month. During our monitoring in the Bhote Koshi catchment, this transition happened around the meteorological monsoon onset and after 400–600 mm of cumulative precipitation over a period of some weeks, but elsewhere it may occur with a greater offset. We note that the similar threshold behavior observed in the rock moisture reservoir on a hillslope in the Northern California Coast Ranges may not be as dependent on transpirative loss, as the onset of groundwater storage happened at a constant cumulative precipitation total for each recorded year in that study (Rempe & Dietrich, 2014). Moreover, within one landscape, the decoupled-to-coupled transition may not be uniform, with locations with less vegetation and soil cover, more precipitation, or less evaporation transitioning sooner.

These findings have likely implications for the prediction of natural hazards in the Himalayas. A precipitation event that may have little impact early in the year, when subsurface moisture is depleted and has a buffering capacity, could result in a flood later in the year when the vadose zone is at field capacity and both infiltration and direct runoff lead to water discharge. Monitoring of subsurface moisture and dv/v can help identify the transition from the decoupled to the coupled state, when the likelihood of flooding changes. This transition occurs when subsurface moisture ceases to rise and the shallow seismic velocity starts to decrease. Similarly, the decoupled-to-coupled transition may also have an impact on deep-seated landsliding: a substantial and sustained hazard in the Himalaya. Such landslides are often attributed to increased pore pressure (Iverson, 2000), which occurs once the vadose zone of the upslope area has reached field capacity. The hydrological regimes highlighted in our study could help delineate a landslide season, during which slope stability is a direct function of local precipitation (Gabet et al., 2004). A universal relation between precipitation rate and landsliding does not apply where the groundwater is episodically decoupled from precipitation input.

Our results also imply that prediction of mountain water resources requires knowledge of the thickness and properties of the soil and regolith layer, which is a gate keeper to the fractured crystalline bedrock in which the groundwater reservoir is primarily located (Rempe & Dietrich, 2014, 2018). During our 3-year observation period, pre-monsoon precipitation did not contribute significantly to discharge but was rather mostly consumed in the vadose zone. However, this period contributes to the wetting of the landscape and preconditions rapid and effective transfer into groundwater and hence river discharge. The moisture content of the vadose zone determines first-order features of the precipitation-discharge relation in the Bhote Koshi catchment, and probably other catchments in the Himalayas and other mountain belts. The modulation cycle exerted by the subsurface moisture shows an indirect relation between precipitation and groundwater that may be responsible for the low streamflow sensitivity to water storage observed in other mountainous areas (Berghuijs et al., 2016). It is mediated not only by the infiltration of rain water, but also by upward water losses due to evaporation and transpiration. The balance of these gains and losses is likely highly sensitive to ecosystem composition, land use and the macroporosity of the soil: parameters that are influenced by climate change (Hirmas et al., 2018; Samaniego et al., 2018).

Recent work by Brunello et al. (2020) highlighted increasing pre-monsoon precipitation totals over the last ~70 years. In conjunction with our findings, a longer and wetter pre-monsoon season would impact directly on the saturation of the vadose zone, the recharge of groundwater and river discharge, increasing the availability of water for hydropower and irrigation purposes. The demand for this water availability is large in densely populated Asian basins, particularly the ones relying on Himalayan freshwater (Immerzeel et al., 2020). Forecasts of global climate change impacts on the Himalayan region predict a reduction of melt-water availability for an estimated 60 million people downstream (Immerzeel et al., 2010). However, if global climate change will also alter the intensity distribution of the Indian monsoon, then we can expect vegetation activity, soil formation, erosion, and subsurface moisture dynamics to change as a consequence, with potentially even more severe consequences for water resources. The effect of subsurface changes due to climate change or changing land use has been acknowledged as a major knowledge gap in the freshwater

resources IPCC special report (Jiménez Cisneros et al., 2015). For instance, decreasing trends in soil moisture due to warmer days (Fischer et al., 2011; A. Wang et al., 2011) would lead to a poor conversion of precipitation to water availability in environments similar to our study area. Therefore, the notion of mountain water towers in the Himalayas and sustainability studies on high mountain areas (Regine Hock, 2019) must be expanded from the cryosphere to include mountain subsurface moisture and groundwater and their complex link with precipitation. With ∼1.5 billion people on Earth projected to rely on discharge sourced from mountain areas (Viviroli et al., 2020), constraining this link for the major lithologies and ecosystems and monitoring the state of the vulnerable vadose zone in mountain regions are keys to anticipating the future trajectories of some of our most important freshwater reserves.

Appendix A: Ambient Noise Processing

Appendix A01: Preprocessing and Calculation of Correlation Functions

A first step of preprocessing is needed to reduce the impact of high amplitude signals such as those induced by earthquakes or rockfalls before calculating the correlation functions. The seismic traces were trimmed to one hour segments, downsampled to 50 Hz, detrended and filtered in the 4–8 Hz frequency range. Then we applied spectral whitening: all the amplitudes in the Fourier spectrum were set to 1 before applying the inverse Fourier transform. The correlation functions with single station cross correlation (SC, Hobiger et al., 2014) were calculated as follows:

$$C_{k_1,k_2}(t_i,\tau) = \int_{t_i-T/2}^{t_i+T/2} \mathrm{sgn}[X_{k_1}(t')] \cdot \mathrm{sgn}[X_{k_2}(t'+\tau)]dt' \tag{A1}$$

In the equation, k_m represents the different components $m = Z, N, E$ with $k_1 \neq k_2$ for SC, t is the time of the year, and τ is the lag time of the correlation. T is the temporal discretization in the correlation process. The sgn function stands for the 1-bit normalization of our signal: positive amplitudes are set to 1 and negative amplitudes are set to −1. We computed correlation functions at a time step of one hour and averaged them on a daily basis in order to get daily correlation functions (DCFs). We stored all the DCFs in a correlation matrix as shown in Figure S2.

Appendix A02: Estimating Velocity Changes

If we assume a spatially homogeneous relative velocity change $\delta v = dv/v$ in the medium, a relative time delay $\delta\tau = dt/\tau$ will be observed in the DCFs coda with $\delta v = -\delta\tau$ where τ is the lapse time in the correlation functions and dt is the absolute time shift of a coherent phase. The relative velocity change has been estimated using the stretching technique (Sens-Schönfelder & Brenguier, 2019).

Depending on the daily velocity change, each DCFs ($C(t_i, \tau)$) will be stretched or compressed and compared to a long term average reference $\xi(\tau)$. For this study, we used multiple references $\xi_r(\tau)$ to avoid the possible degradation of a unique reference when averaged over the whole time period (Sens-Schönfelder et al., 2014). To do so, we first computed monthly references $\xi_r(\tau)$ with an overlap of 15 days. For each of these references, we calculated the correlation coefficients $R_r(t_i, \varepsilon_j)$ between stretched versions of the reference and the DCF as

$$R_r(t_i,\varepsilon_j) = \int_{\tau_1}^{\tau_2} C(t_i,\tau)\xi_r(\tau(1+\varepsilon_j))\mathrm{d}\tau \tag{A2}$$

where τ is the traveltime of waves in the DCF and ε_j indicates a set of stretch-values that are tested in the time window set by $[\tau_1, \tau_2]$. We defined the length of the time window as follows: we skipped four signal periods before computing the stretching on a duration of 12 periods (corresponding window indicated on Figure S2). One period corresponds to the lowest frequency of the filter we previously applied (here $\tau_1 = 1$ s). Introducing τ_1 is necessary to avoid the use of early arrivals that are prone to change in noise sources characteristics. All $R_r(t_i, \varepsilon_j)$ values were stored in a similarity matrix as shown in Figure S3.

For each reference, a first daily measurement of $\delta v(t_i)$ can be done by reading the amount of stretching ε_j that yields the daily maximum $R_r(t_i, \varepsilon_j)$ value. To combine the measurements done with the multiple references, we stacked all similarity matrices $R_r(t_i, \varepsilon_j)$ after correcting for their shifting due to the velocity differences between the references. We finally obtained a stacked similarity matrix $R(t_i, \varepsilon_j)$ which describes the daily velocity variations obtained from one combination of sensor components k_1, k_2 (Figure S3).

We applied this method to the three possible combinations (ZN, ZE, EN). In a last step, we stacked the three $R(t_i, \varepsilon_j)$ matrices and picked the ε_j as the location of the maximum of $R(t_i, \varepsilon_j)$ again. The final daily $\delta v(t_i)$ at the station is equal to ε_j.

Appendix B: Modeling Velocity Changes Induced by Groundwater Level Variations, Detailed Method

Appendix B01: Model A

The first applied model in the paper is similar to the one used in Sens-Schönfelder and Wegler (2006) and Hillers et al. (2014). In a first step, we model the evolution of the groundwater table depth. Conventions are shown on Figure 3 of the main text. The variation of the hydraulic head is here approximated as a representative column reservoir of porosity ϕ. We assume that the rate of recession of the hydraulic head $h(t)$ is proportional to its height such as

$$\frac{dh}{dt}(t) = \frac{P(t)}{\phi} - ah(t) \tag{B1}$$

where $P(t)$ is the precipitation rate and is the decay parameter. Similarly to an unconfined aquifer that obeys to Darcy's law, this equation predicts an exponential decay of the hydraulic head after impulsive rain events at t_n with its analytical solution:

$$h(t - t_n) = \frac{P(t_n)}{\phi} e^{-a(t-t_n)} \tag{B2}$$

We introduce the asymptotic level h_0 to convert the hydraulic head height into the absolute groundwater table depth GWD(t) as shown on Figure 3 with:

$$GWD(t) = h_0 + h(t) \tag{B3}$$

Equation B1 is here discretized and integrated using a central Euler scheme with the daily precipitation data as inputs to obtain daily $h(t)$. Figure S4a shows examples of the model using our precipitation data set with parameters taken as $\phi = 0.017$ and $a = 0.08$ d^{-1}. Because absolute groundwater level changes are unconstrained, we run our simulations with an arbitrary but realistic value of $h_0 = -50$ m.

We then convert the hydraulic head daily variations $h(t)$ into daily relative velocity changes δv. We assume that a change of $h(t)$ will induce a change in the relative slowness profile $S(t, z)$ with δs being the relative slowness difference between the saturated and dry state of the reservoir. We define a reference hydraulic head h_{ref} that is taken as the mean $h(t)$ over the whole time period of the study. We have $S(t, z) = \delta s$ for $h(t) < z < h_{\text{ref}}$ and $S(t, z) = -\delta s$ for $h_{\text{ref}} < z < h(t)$.

To model the depth sensitivity of the seismic waves, we used the 3-D scattered wavefield kernel derived by Pacheco and Snieder (2005). Because we applied the single station cross correlation technique, we considered coincident source and receiver which leads to the following equation

$$K_{3D}\left(\mathbf{x}, \tau\right) = (2\pi Dr)^{-1} \exp\frac{-r^2}{D\tau} \tag{B4}$$

with D being the diffusion constant, $\mathbf{x}$ is the point in space at distance $\mathbf{r}$ from the source/receiver and τ is the lapse time in the correlation function. We horizontally integrate $K_{3D}(\mathbf{x}, \tau)$ to get the depth sensitivity $K(z, \tau)$. Kernel examples for different diffusivity constant are plotted in Figure S4b.

In a last step, we compute the daily delay time by integrating the slowness perturbation profile weighted by the kernel as

$$\delta\tau(t,\tau) = \int_0^\infty S(t,z)K(z,\tau)dz. \tag{B5}$$

We then convert the delay times in modeled daily relative velocity changes $\delta v_m = -\delta\tau/\tau$. We report in Figure S4c different synthetic velocity changes obtained from Equation 10 with the 3 kernels proposed in Figure S4b. Because the kernels do not change significantly at the spatial scale of groundwater changes (~10 m) results are poorly dependent on the value of the diffusivity D and the kernel used. Therefore, we use the value of $D = 1.10^5$ m^2 s^{-1} for our simulations.

We used an interior point algorithm in Matlab® (fmincon) to minimize the following least square misfit between our model and the data over the total number of days N:

$$\text{misfit} = \sum_{i=1}^{N}(\delta v_m(i) - \delta v(i))^2. \tag{B6}$$

Our best fitting model is obtained with $a = 0.0134$ d^{-1}, $\phi = 0.032$, and $\delta s = 0.007$. We note that different combinations for ϕ and δs can give similar results.

Appendix B02: Model B

As explained in the main text, we propose to implement the role of the subsurface moisture reservoir with a simple antecedent precipitation index approach that does not require unconstrained physical parameters. The antecedent index is computed as follows:

$$P_M(t) = P_M(t-1)\exp(\ln 0.5 \,/\, M) + R_h(t)\exp(\ln 0.5 \,/\, 2M). \tag{B7}$$

$R_h(t)$ is the cumulative precipitation from $t-1$ to t and M is the half-time period in days required for the precipitation fed to the layer to decay to half of its initial value. We then introduce a threshold P_θ to model the field capacity of the subsurface: precipitation is only passed to the groundwater storage when $P_M(t) > P_\theta$. We calculate the P_θ threshold as the mean value of $P_M(t)$ at the date of the June 17, 2016, June 21, 2017, and June 9, 2018 (red lines on Figures S5b–S5f). We chose these dates based on the trend detection of the onset of the seismic velocity decrease and the plateau observed in the soil moisture data that defines the start of the coupled regime. Then, we model the effect of vegetation in introducing the parameter h_b which is the critical depth at which the vegetation do not influence the drainage of groundwater anymore (see conventions in Figure 3). For this study we take the value of $h_b = 10$ m which is a classic reported tree root depth (Canadell et al., 1996). We introduce the effect of transpiration on the groundwater with a second term to Equation B1 involving an additional scaling term b within the depth h_b. Therefore, for $P_M(t) > P_\theta$, we have

$$\frac{dh}{dt} = \frac{P(t)}{\phi} - a\,(GWD(t) - h_0) - b\,(\min(0, GWD(t) - h_b)). \tag{B8}$$

For periods when groundwater is not connected to the surface ($P_M(t) < P_\theta$), we have

$$\frac{dh}{dt} = -a\,(GWD(t) - h_0). \tag{B9}$$

We convert the hydraulic head $h(t)$ evolution in seismic velocity variations following the same method described in model **A**. We test a whole class of models with parameter M ranging from 1 to 100 days and try to fit the data in minimizing Equation B6 using the same solver applied before for model **A**. The corresponding misfit values are shown in Figure S5a. The misfit space shows several local minima ranging from $M \sim 10$ days to $M \sim 40$ days. This suggests that values corresponding to the weekly and monthly scale fit the data equally well. We show five inverted models in Figures S5b–S5f and their corresponding antecedent precipitation index P_M.

Conflict of Interest

The authors declare no conflicts of interest relevant to this study.

Data Availability Statement

Data have been uploaded at the following repositories: seismic data (DOI: 10.14470/KA7560056170), Kahule Khola hydrometric data (DOI: 10.5880/GFZ.4.6.2021.003), weather stations data (DOI: 10.5880/GFZ.4.6.2021.003).

Acknowledgments
This work was supported by the GFZ HART program. The authors are grateful to Bhairab Sitaula and all the HART Nepal team for their work on the field. The authors also thank one anonymous reviewer and Douglas Burbank for their valuable feedback that improved considerably the clarity of the paper. Open access funding enabled and organized by Projekt DEAL.

References

Alley, W. M., Healy, R. W., LaBaugh, J. W., & Reilly, T. E. (2002). Flow and storage in groundwater systems. *Science*, *296*(5575), 1985–1990. https://doi.org/10.1126/SCIENCE.1067123

Andermann, C., Longuevergne, L., Bonnet, S., Crave, A., Davy, P., & Gloaguen, R. (2012). Impact of transient groundwater storage on the discharge of Himalayan rivers. *Nature Geoscience*, *5*, 127–132. https://doi.org/10.1038/NGEO1356

Berghuijs, W. R., Hartmann, A., & Woods, R. A. (2016). Streamflow sensitivity to water storage changes across Europe. *Geophysical Research Letters*, *43*(5), 1980–1987. https://doi.org/10.1002/2016GL067927

Bookhagen, B., & Burbank, D. W. (2010). Toward a complete Himalayan hydrological budget: Spatiotemporal distribution of snowmelt and rainfall and their impact on river discharge. *Journal of Geophysical Research*, *115*(3). https://doi.org/10.1029/2009JF001426

Brenguier, F., Campillo, M., Hadziioannou, C., Shapiro, N. M., Nadeau, R. M., & Larose, E. (2008). Postseismic relaxation along the San Andreas fault at Parkfield from continuous seismological observations. *Science*, *321*(5895), 1478–1481. https://doi.org/10.1126/science.1160943

Brunello, C. F., Andermann, C., Helle, G., Comiti, F., Tonon, G., Tiwari, A., & Hovius, N. (2019). Hydroclimatic seasonality recorded by tree ring δ18O signature across a Himalayan altitudinal transect. *Earth and Planetary Science Letters*, *518*, 148–159. https://doi.org/10.1016/J.EPSL.2019.04.030

Brunello, C. F., Andermann, C., Marc, O., Schneider, K. A., Comiti, F., Achleitner, S., & Hovius, N. (2020). Annually resolved monsoon onset and withdrawal dates across the Himalayas derived from local precipitation statistics. *Geophysical Research Letters*, *47*. https://doi.org/10.1029/2020GL088420

Canadell, J., Jackson, R. B., Ehleringer, J. B., Mooney, H. A., Sala, O. E., & Schulze, E.-D. (1996). Maximum rooting depth of vegetation types at the global scale. *Oecologia*, *108*(4), 583–595. https://doi.org/10.1007/BF00329030

Clements, T., & Denolle, M. A. (2018). Tracking groundwater levels using the ambient seismic field. *Geophysical Research Letters*, *45*(13), 6459–6465. https://doi.org/10.1029/2018GL077706

Condon, L. E., Atchley, A. L., & Maxwell, R. M. (2020). Evapotranspiration depletes groundwater under warming over the contiguous United States. *Nature Communications*, *11*(1). https://doi.org/10.1038/s41467-020-14688-0

DiCarlo, D. A. (2004). Experimental measurements of saturation overshoot on infiltration. *Water Resources Research*, *40*(4). https://doi.org/10.1029/2003WR002670

DiCarlo, D. A. (2006). Quantitative network model predictions of saturation behind infiltration fronts and comparison with experiments. *Water Resources Research*, *42*(7). https://doi.org/10.1029/2005WR004750

Dralle, D. N., Hahm, W. J., Rempe, D. M., Karst, N. J., Thompson, S. E., & Dietrich, W. E. (2018). Quantification of the seasonal hillslope water storage that does not drive streamflow. *Hydrological Processes*, *32*(13), 1978–1992. https://doi.org/10.1002/hyp.11627

Fischer, T., Gemmer, M., Lüliu, L., & Buda, S. (2011). Temperature and precipitation trends and dryness/wetness pattern in the Zhujiang River Basin, South China, 1961-2007. *Quaternary International*, *244*(2), 138–148. https://doi.org/10.1016/j.quaint.2010.08.010

Gabet, E. J., Burbank, D. W., Putkonen, J. K., Pratt-Sitaula, B. A., & Ojha, T. (2004). Rainfall thresholds for landsliding in the Himalayas of Nepal. *Geomorphology*, *63*(3–4), 131–143. https://doi.org/10.1016/J.GEOMORPH.2004.03.011

Gassenmeier, M., Sens-Schönfelder, C., Delatre, M., & Korn, M. (2015). Monitoring of environmental influences on seismic velocity at the geological storage site for CO2 in Ketzin (Germany) with ambient seismic noise. *Geophysical Journal International*, *200*(1), 524–533. https://doi.org/10.1093/gji/ggu413

Gassenmeier, M., Sens-Schönfelder, C., Eulenfeld, T., Bartsch, M., Victor, P., Tilmann, F., & Korn, M. (2016). Field observations of seismic velocity changes caused by shaking-induced damage and healing due to mesoscopic nonlinearity. *Geophysical Journal International*, *204*(3), 1490–1502. https://doi.org/10.1093/gji/ggv529

Gleeson, T., Befus, K. M., Jasechko, S., Luijendijk, E., & Cardenas, M. B. (2016). The global volume and distribution of modern groundwater. *Nature Geoscience*, *9*(2), 161–167. https://doi.org/10.1038/ngeo2590

Gleeson, T., Novakowski, K., & Kurt Kyser, T. (2009). Extremely rapid and localized recharge to a fractured rock aquifer. *Journal of Hydrology*, *376*(3–4), 496–509. https://doi.org/10.1016/j.jhydrol.2009.07.056

Helle, H. B., Pham, N. H., & Carcione, J. M. (2003). Velocity and attenuation in partially saturated rocks: Poroelastic numerical experiments. *Geophysical Prospecting*, *51*(6), 551–566. https://doi.org/10.1046/j.1365-2478.2003.00393.x

Hillers, G., Campillo, M., & Ma, K.-F. (2014). Seismic velocity variations at TCDP are controlled by MJO driven precipitation pattern and high fluid discharge properties. *Earth and Planetary Science Letters*, *391*, 121–127. https://doi.org/10.1016/J.EPSL.2014.01.040

Hirmas, D. R., Giménez, D., Nemes, A., Kerry, R., Brunsell, N. A., & Wilson, C. J. (2018). Climate-induced changes in continental-scale soil macroporosity may intensify water cycle. *Nature*, *561*(7721), 100–103. https://doi.org/10.1038/s41586-018-0463-x

Hobiger, M., Wegler, U., Shiomi, K., & Nakahara, H. (2014). Single-station cross-correlation analysis of ambient seismic noise: Application to stations in the surroundings of the 2008 Iwate-Miyagi Nairiku earthquake. *Geophysical Journal International*, *198*(1), 90–109. https://doi.org/10.1093/gji/ggu115

Ichii, K., Kawabata, A., & Yamaguchi, Y. (2010). Global correlation analysis for NDVI and climatic variables and NDVI trends: 1982-1990. *International Journal of Remote Sensing*, *23*, 3873–3878. https://doi.org/10.1080/01431160110119416

Immerzeel, W. W., Lutz, A. F., Andrade, M., Bahl, A., Biemans, H., Bolch, T., et al. (2020). Importance and vulnerability of the world's water towers. *Nature*, *577*(7790), 364–369. https://doi.org/10.1038/s41586-019-1822-y

Immerzeel, W. W., Van Beek, L. P. H., & Bierkens, M. F. P. (2010). Climate change will affect the asian water towers. *Science*, *328*, 1382–1385. https://doi.org/10.1126/science.1183188

Iverson, R. M. (2000). Landslide triggering by rain infiltration. *Water Resources Research*, *36*(7), 1897–1910. https://doi.org/10.1029/2000WR900090

Jasechko, S., Kirchner, J. W., Welker, J. M., & McDonnell, J. J. (2016). Substantial proportion of global streamflow less than three months old. *Nature Geoscience*, *9*(2), 126–129. https://doi.org/10.1038/ngeo2636

Jiménez Cisneros, B. E., Oki, T., Arnell, N. W., Benito, G., Cogley, J. G., Döll, P., et al. (2015). *Freshwater resources: Climate change 2014 impacts, adaptation and vulnerability: Part A: Global and sectoral aspects* (pp. 229–270). https://doi.org/10.1017/CBO9781107415379.008

Katsura, S. y., Kosugi, K. i., Mizutani, T., Okunaka, S., & Mizuyama, T. (2008). Effects of bedrock groundwater on spatial and temporal variations in soil mantle groundwater in a steep granitic headwater catchment. *Water Resources Research*, *44*(9). https://doi.org/10.1029/2007WR006610

Kim, D., & Lekic, V. (2019). Groundwater variations from autocorrelation and receiver functions. *Geophysical Research Letters*, *46*, 13722–13729. https://doi.org/10.1029/2019GL084719

Koirala, S., Jung, M., Reichstein, M., de Graaf, I. E. M., Camps-Valls, G., Ichii, K., et al. (2017). Global distribution of groundwater-vegetation spatial covariation. *Geophysical Research Letters*, *44*(9), 4134–4142. https://doi.org/10.1002/2017GL072885

Kosugi, K. i., Katsura, S. y., Mizuyama, T., Okunaka, S., & Mizutani, T. (2008). Anomalous behavior of soil mantle groundwater demonstrates the major effects of bedrock groundwater on surface hydrological processes. *Water Resources Research*, *44*(1). https://doi.org/10.1029/2006WR005859

Lecocq, T., Longuevergne, L., Pedersen, H. A., Brenguier, F., & Stammler, K. (2017). Monitoring ground water storage at mesoscale using seismic noise: 30 years of continuous observation and thermo-elastic and hydrological modeling. *Scientific Reports*, *7*(1). https://doi.org/10.1038/s41598-017-14468-9

Lobkis, O. I., & Weaver, R. L. (2001). On the emergence of the Green's function in the correlations of a diffuse field. *Journal of the Acoustical Society of America*, *110*(6), 3011–3017. https://doi.org/10.1121/1.1417528

Maxwell, R. M., & Condon, L. E. (2016). Connections between groundwater flow and transpiration partitioning. *Science*, *353*(6297), 377–380. https://doi.org/10.1126/science.aaf7891

McGuire, K. J., & McDonnell, J. J. (2006). A review and evaluation of catchment transit time modeling. *Journal of Hydrology*, *330*(3–4), 543–563. https://doi.org/10.1016/j.jhydrol.2006.04.020

Montgomery, D. R., Dietrich, W. E., Torres, R., Anderson, S. P., Heffner, J. T., & Loague, K. (1997). Hydrologic response of a steep, unchanneled valley to natural and applied rainfall. *Water Resources Research*, *33*(1), 91–109. https://doi.org/10.1029/96WR02985

Müller, M. F., Dralle, D. N., & Thompson, S. E. (2014). Analytical model for flow duration curves in seasonally dry climates. *Water Resources Research*, *50*(7), 5510–5531. https://doi.org/10.1002/2014WR015301

Obermann, A., Planès, T., Larose, E., Sens-Schönfelder, C., & Campillo, M. (2013). Depth sensitivity of seismic coda waves to velocity perturbations in an elastic heterogeneous medium. *Geophysical Journal International*, *194*(1), 372–382. https://doi.org/10.1093/gji/ggt043

Oki, T., & Kanae, S. (2006). Global hydrological cycles and world water resources. *Science*, *313*(5790), 1068–1072. https://doi.org/10.1126/SCIENCE.1128845

Onda, Y. (1989). Influence of water storage capacity in regolith zone on runoff characteristics and slope failure on granitic hills in Aichi, Japan. *Transactions—Japanese Geomorphological Union*, *10*(1), 13–26.

Pacheco, C., & Snieder, R. (2005). Time-lapse travel time change of multiply scattered acoustic waves. *Journal of the Acoustical Society of America*, *118*(3), 1300–1310. https://doi.org/10.1121/1.2000827

Padilla, C., Onda, Y., & Iida, T. (2015). Interaction between runoff-bedrock groundwater in a steep headwater catchment underlain by sedimentary bedrock fractured by gravitational deformation. *Hydrological Processes*, *29*(20), 4398–4412. https://doi.org/10.1002/hyp.10498

Padilla, C., Onda, Y., Iida, T., Takahashi, S., & Uchida, T. (2014). Characterization of the groundwater response to rainfall on a hillslope with fractured bedrock by creep deformation and its implication for the generation of deep-seated landslides on Mt. Wanitsuka, Kyushu Island. *Geomorphology*, *204*, 444–458. https://doi.org/10.1016/j.geomorph.2013.08.024

Putkonen, J. K. (2004). Continuous snow and rain data at 500 to 4400 m altitude near Annapurna, Nepal, 1999-2001. *Arctic, Antarctic, and Alpine Research*, *36*(2), 244–248. https://doi.org/10.1657/1523-0430(2004)036[0244:csarda]2.0.co;2

Regine Hock, G. R. (2019). High mountain areas. *IPCC SR Ocean and Cryosphere*, *4*(1), 1–96.

Rempe, D. M., & Dietrich, W. E. (2014). A bottom-up control on fresh-bedrock topography under landscapes. *Proceedings of the National Academy of Sciences of the United States of America*, *111*(18), 6576–6581. https://doi.org/10.1073/pnas.1404763111

Rempe, D. M., & Dietrich, W. E. (2018). Direct observations of rock moisture, a hidden component of the hydrologic cycle. *Proceedings of the National Academy of Sciences of the United States of America*, *115*(11), 2664–2669. https://doi.org/10.1073/pnas.1800141115

Renée Brooks, J., Barnard, H. R., Coulombe, R., & McDonnell, J. J. (2010). Ecohydrologic separation of water between trees and streams in a Mediterranean climate. *Nature Geoscience*, *3*(2), 100–104. https://doi.org/10.1038/ngeo722

Richter, T., Sens-Schönfelder, C., Kind, R., & Asch, G. (2014). Comprehensive observation and modeling of earthquake and temperature-related seismic velocity changes in northern Chile with passive image interferometry. *Journal of Geophysical Research: Solid Earth*, *119*(6), 4747–4765. https://doi.org/10.1002/2013JB010695

Running, S. W., & Nemani, R. R. (1988). Relating seasonal patterns of the AVHRR vegetation index to simulated photosynthesis and transpiration of forests in different climates. *Remote Sensing of Environment*, *24*(2), 347–367. https://doi.org/10.1016/0034-4257(88)90034-X

Salve, R., Rempe, D. M., & Dietrich, W. E. (2012). Rain, rock moisture dynamics, and the rapid response of perched groundwater in weathered, fractured argillite underlying a steep hillslope. *Water Resources Research*, *48*(11), 1–25. https://doi.org/10.1029/2012WR012583

Samaniego, L., Thober, S., Kumar, R., Wanders, N., Rakovec, O., Pan, M., et al. (2018). Anthropogenic warming exacerbates European soil moisture droughts. *Nature Climate Change*, *8*(5), 421–426. https://doi.org/10.1038/s41558-018-0138-5

Sens-Schönfelder, C., & Brenguier, F. (2019). Noise-based monitoring. In N. Nakata, L. Gualtieri, & A. Fichtner (Eds.), *Seismic ambient noise* (pp. 267–301). Cambridge University Press.

Sens-Schönfelder, C., Pomponi, E., & Peltier, A. (2014). Dynamics of Piton de la Fournaise volcano observed by passive image interferometry with multiple references. *Journal of Volcanology and Geothermal Research*, *276*, 32–45. https://doi.org/10.1016/J.JVOLGEORES.2014.02.012

Sens-Schönfelder, C., & Wegler, U. (2006). Passive image interferometry and seasonal variations of seismic velocities at Merapi Volcano, Indonesia. *Geophysical Research Letters*, *33*(21). https://doi.org/10.1029/2006GL027797

Taktikou, E., Bourazanis, G., Papaioannou, G., & Kerkides, P. (2016). Prediction of soil moisture from remote sensing data. *Procedia Engineering*, *162*, 309–316. https://doi.org/10.1016/J.PROENG.2016.11.066

Tani, M. (1997). Runoff generation processes estimated from hydrological observations on a steep forested hillslope with a thin soil layer. *Journal of Hydrology*, *200*(1–4), 84–109. https://doi.org/10.1016/S0022-1694(97)00018-8

Tipper, E. T., Bickle, M. J., Galy, A., West, A. J., Pomiès, C., & Chapman, H. J. (2006). The short term climatic sensitivity of carbonate and silicate weathering fluxes: Insight from seasonal variations in river chemistry. *Geochimica et Cosmochimica Acta*, *70*(11), 2737–2754. https://doi.org/10.1016/j.gca.2006.03.005

Viviroli, D., Dürr, H. H., Messerli, B., Meybeck, M., & Weingartner, R. (2007). Mountains of the world, water towers for humanity: Typology, mapping, and global significance. *Water Resources Research*, *43*(7). https://doi.org/10.1029/2006WR005653

Viviroli, D., Kummu, M., Meybeck, M., Kallio, M., & Wada, Y. (2020). Increasing dependence of lowland populations on mountain water resources. *Nature Sustainability*, *3*(11), 917–928. https://doi.org/10.1038/s41893-020-0559-9

Wang, A., Lettenmaier, D. P., & Sheffield, J. (2011). Soil moisture drought in China, 1950-2006. *Journal of Climate*, *24*(13), 3257–3271. https://doi.org/10.1175/2011JCLI3733.1

Wang, Q.-Y., Brenguier, F., Campillo, M., Lecointre, A., Takeda, T., & Aoki, Y. (2017). Seasonal crustal seismic velocity changes throughout Japan. *Journal of Geophysical Research: Solid Earth*, *122*(10), 7987–8002. https://doi.org/10.1002/2017JB014307

White, J. E. (1975). Computed seismic speeds and attenuation in rocks with partial gas saturation. *Geophysics*, *40*(2), 224–232. https://doi.org/10.1190/1.1440520

Zillgens, B., Merz, B., Kirnbauer, R., & Tilch, N. (2007). Analysis of the runoff response of an alpine catchment at different scales. *Hydrology and Earth System Sciences*, *11*(4), 1441–1454. https://doi.org/10.5194/hess-11-1441-2007